Laser-induced interference, focusing, and diffraction of rescattering molecular photoelectrons

Yurchenko, S. N.; Patchkovskii, S.; Litvinyuk, I. V.; Corkum, P. B.; Yudin, G. L.

Publisher's version / Version de l'éditeur:
https://doi.org/10.1103/PhysRevLett.93.223003
Physical Review Letters, 93, 22, pp. 223003-1-223003-4, 2004-11-23

Laser-Induced Interference, Focusing, and Diffraction of Rescattering Molecular Photoelectrons

S. N. Yurchenko,[1] S. Patchkovskii,[1] I.V. Litvinyuk,[1,2] P. B. Corkum,[1] and G. L. Yudin[1,3,*]

[1]*National Research Council of Canada, Ottowa, Ontario K1A 0R6, Canada*

[2]*J.R. Macdonald Laboratory, Kansas State University, Manhattan, Kansas 66506, USA*

[3]*Laboratoire de Chimie Théorique, Université de Sherbrooke, Sherbrooke, Québec J1K 2R1, Canada*

(Received 29 March 2004; published 23 November 2004)

We solve the time-dependent Schrödinger equation in three dimensions for H_2^+ in a one-cycle laser pulse of moderate intensity. We consider fixed nuclear positions and Coulomb electron-nuclear interaction potentials. We analyze the field-induced electron interference and diffraction patterns. To extract the ionization dynamics we subtract the excitations to low-lying bound states explicitly. We follow the time evolution of a well-defined wave packet that is formed near the first peak of the laser field. We observe the fragmentation of the wave packet due to molecular focusing. We show how to retrieve a diffraction molecular image by taking the ratio of the momentum distributions in the two lateral directions. The positions of the diffraction peaks are well described by the classical double slit diffraction rule.

DOI: 10.1103/PhysRevLett.93.223003 PACS numbers: 32.80.Rm

In the simplest textbook case, diffraction of a monochromatic plane wave on a double slit, the diffraction pattern is determined by the slit separation R and the wavelength λ. Constructive interference occurs when the condition

$$\sin\theta = (\lambda/R)m, m = 0, 1, 2, \ldots \quad (1)$$

is satisfied where θ is the angle between the direction of wave propagation and the direction to the detector. In the case of electron diffraction, λ is the de Broglie electron wavelength $\lambda\!\!\!^{-}_e = 2\pi/p_e e$, where p_e is the electron momentum (unless stated otherwise, atomic units $e = m_e = \hbar = 1$ are used). For a photoionized electron, the recollision momentum distribution is very broad, with the effective maximum electron momentum $p_{\max}$ corresponding to $\lambda\!\!\!^{-}_{\text{eff}} = 2\pi/p_{\max}$. The laser field and the molecular potential both affect $p_{\max}$.

In contrast to diffraction of a free-electron wave packet, we observe that for laser-induced electron diffraction, the clear spatial picture is obscured. We introduce a new method for detecting laser-induced electron diffraction by observing the ratio of two lateral photoelectron distributions. Viewed in this way, laser-induced electron diffraction is as simple as optical diffraction [Eq. (1)]. The number of diffraction peaks is determined by the value $\lambda\!\!\!^{-}_{\text{eff}}/R$.

In atomic physics, laser-induced electron rescattering has been important since a simple semiclassical model of high harmonic generation was proposed [1]. In this model, the oscillations of a photoelectron in the laser field lead to recombination with emission of high-energy photons. The electric-field of the parent atomic ion focuses electron trajectories. Focusing increases the correlation between the photoelectron and bound electrons (''Coulomb focusing'' [2,3]).

In the molecular case, electron rescattering is complicated by the multicenter nature of the ion-electron potential and by nuclear dynamics. However, it has been proposed that multicenter electron rescattering contains diffractive information and therefore provides a technique for probing ultrafast molecular dynamics [4,5]. Exploring the feasibility of laser-induced electron diffraction is our motivation. We study diffraction using a H_2^+ molecular ion. Recently, molecular interference and diffraction in H_2^+ was demonstrated in two-dimensional (2D) simulations of strong-field ionization [6] and three-dimensional (3D) calculations of high harmonics generation [7]. An analytical and 2D numerical analysis in the tunneling regime focusing on unmasking diffraction patterns for each recollision energy is reported in Ref. [8]. We present a 3D numerical simulation of interference, focusing, and diffraction of rescattering molecular photoelectrons in moderate laser fields.

Two advances in experimental technology make laser-induced electron diffraction feasible. Motivated by the generation and characterization of attosecond pulses [9], experimentalists have learned to produce intense, phase-controlled few-optical cycle pulses [10]. Already few-cycle pulses are being used for molecular experiment [11]. Motivated by the need to align molecules in the laboratory frame, experimentalists have developed adiabatic [12] and nonadiabatic [13,14] alignment methods. Strong-field experiments are already performed on aligned molecules [15].

Diffraction effects are most prominent for molecules aligned perpendicular to the laser polarization [4]. Here we only consider this intrinsically 3D case. In our model, the H_+^2 molecular ion is aligned along the x axis in Cartesian space with internuclear separation $R = 6$. Although we only show the results for $R = 6$, our general

conclusions apply to all values of R. The laser electric field $\vec{E}(t) = \vec{E}_0 \sin(\omega t)$ is parallel to the z axis. We choose the frequency ω to correspond to the wavelength of 400 nm. The field is turned on at $t = 0$ and turned off at $t = 2\pi/\omega$. Although an artificial pulse, none of its parameters are critical for our conclusions. We choose it to give a clear physical picture of the photoelectron dynamics. We simulate ionization at two moderate laser intensities $I = 10^{14}$ and 3×10^{14} W/cm^2 to study the influence of the recollision electron momentum.

We perform a direct numerical integration of the time-dependent Schrödinger equation in 3D Cartesian space (please see Refs. [16,17] for general methods). We use the electric-field gauge with the electron-laser field interaction potential in the dipole $\vec{r} \cdot \vec{E}(t)$ form. The Laplacian operator is evaluated using the standard three-point finite-difference expression. The electron-nuclear interaction is described by the integral of the Coulomb potential over the elementary volume associated with a grid point. For volume elements away from the point nucleus, the integral is the value of the Coulomb potential at the central point. For volume elements close to one of the nuclei, the value of the integral remains finite. Therefore, no special treatment is required for the Coulomb singularity.

We use time step $\Delta t = 0.002$ together with the "leapfrog" algorithm [18] to describe the time evolution (note: atomic unit of time is $\approx 2.42 \times 10^{-17}$ s). In this approach, the time derivative of the wave function at time t is used to propagate the wave function from time $t - \Delta t$ to time $t + \Delta t$. Although simple, the leapfrog algorithm provides stable, reversible propagation in time. The initial wave function $\Psi(\vec{r}, 0)$ is the ground electronic state $^2\Sigma_g$. The wave function $\Psi(\vec{r}, 0)$ is obtained using Liu's version of the Davidson method [19,20]. The spatial grid ($x = 80$; $y = 80$; $z = 160$) Bohr was chosen to ensure that negligible population reaches the absorbing boundaries. The uniform grid spacing of 0.25 is sufficient to support electron momentum distribution induced by the laser field. We monitor the wave function norm to ensure numerically stable time evolution.

Because of the strong coupling between neighboring volume elements introduced by the finite-difference Laplacian operator, standard diagonal preconditioning techniques [19,20] are not effective for our problem. Instead, we developed a new "kinetic error diffusion" preconditioner. The preconditioner uses a $3 \times 3 \times 3$ wave function stencil chosen to give unit Laplacian at the central point. The values of the Laplacian for all other volume elements affected by the stencil are minimized. For our model the new preconditioner reduces the number of iterations by a factor of 5. For higher excited states we also employ a multiresolution approach where the eigenstates values of the Hamiltonian are first converged on a coarse numerical grid and then subdivided.

Ultrashort laser pulse of moderate intensity can produce large bound, excited state populations that may contaminate the diffraction pattern for short times. Because experiments can only measure unbound electrons, it is essential to subtract from the total wave function $\Psi(\vec{r}, t)$ the contribution of the bound molecular states. The projector

$$\hat{P} = 1 - \sum_n |n\rangle\langle n| \tag{2}$$

includes 33 lowest bound states $|n\rangle$, separated from the continuum by more than 0.15 Ry. Higher, Rydberg-like states will have low lateral momentum and will not contribute to the diffraction pattern. Moreover, at times when $\vec{E}(t) = 0$, the excited state populations become neg-

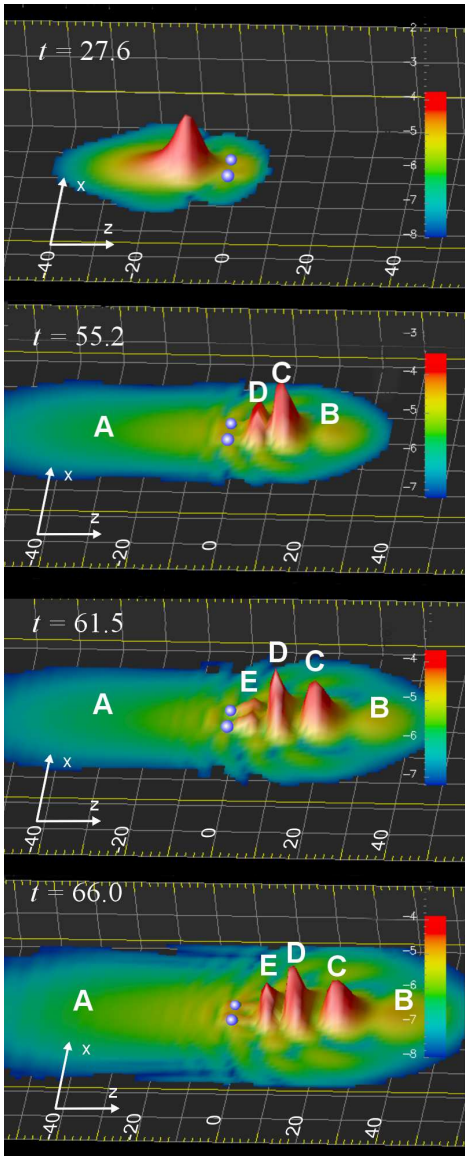

FIG. 1 (color online). The time evolution of the ionized part of the spatial electron density distributions at $I = 3 \times 10^{14}$ W/cm^2. The density slices are in the xz plane. **A** and **B** label directly detached wave packets. **C**, **D**, and **E** label the focused wave packets; see text. The electron density is plotted using a $\log_{10}$ scale.

ligible for $n > 20$. To characterize the dynamics of the 3D wave function $\Psi(\vec{r}, t)$ we use the following reduced metrics: (i) the probability densities in Cartesian and momentum spaces, $|\Psi(\vec{r}, t)|^2$ and $|\Psi(\vec{p}, t)|^2$; (ii) the populations of the bound states, and (iii) the ionization probability.

Images of the ionized part of the electron density are illustrated in Fig. 1 for $I = 3 \times 10^{14}$ W/cm^2. After a half cycle ($t \geq \pi/\omega \approx 27.6$), the velocity distribution of a wide, Gaussian-shaped wave packet exhibits a significant tail at high momenta (see Fig. 2). As a result, the fast part (**A**) of the wave packet in Fig. 1 continues to move away from the nuclei even after the field reverses direction. By the end of the pulse ($t = 2\pi/\omega \approx 55.2$), the maximum of the wave packet has moved through the molecule and the interference pattern becomes prominent.

At low instantaneous laser field, near $t \approx 55.2$ and after the laser pulse, the nuclei focus the slow part of the wave packet forming an interference pattern on the other side of the nuclei. Before $t = 55.2$ the electron is focused into a two-hump electron wave packet. This split wave packet continues moving to the right side and is transformed into a single, longitudinally-compressed wave packet labeled as **C** in Fig. 1. Meanwhile, molecular focusing produces the second two-hump electron wave packet **D**, which also spreads and moves to the right side. During $t \approx 58$–62, the third electron wave packet **E** repeats the same evolution. In addition, a fast small wave packet **B** moves to the right-hand side ahead of the wave packets **C**, **D**, and **E**. This portion of the electron density is formed by tunnel ionization near the time of the second maximum of laser field. Its shape is close to Gaussian. The molecular potential of the nuclei slows it down with little change in shape.

To express the observed diffraction patterns in a quantitative form, we consider the reduced momentum distribution along laser polarization direction, given by

$$\chi_z(p, t) = \int |\Psi(p_x, p_y, p, t)|^2 dp_x dp_y. \quad (3)$$

The distributions at $I = 10^{14}$ and 3×10^{14} W/cm^2 are shown in Fig. 2. The fast edge of $\chi_z(p, t)$ appears at the effective momentum value $p_{\max}$ connected to the de Broglie wavelength λ_{eff} in the diffraction condition. After one cycle, $p_{\max} \approx 1.2$ and ≈ 1.6 at $I = 10^{14}$ and 3×10^{14} W/cm^2, respectively. These values correspond to the maximum momenta of an electron in the combined laser and molecular field. They lead to λ_{eff}/R—ratios of approximately 5/6 and 4/6. Thus, one can expect at least one diffraction maximum for $I = 10^{14}$ W/cm^2 and two for $I = 3 \times 10^{14}$ W/cm^2. Note that without significant contribution to the electron kinetic energy from the molecular potential, diffraction fringes would not form for $I = 10^{14}$ W/cm^2.

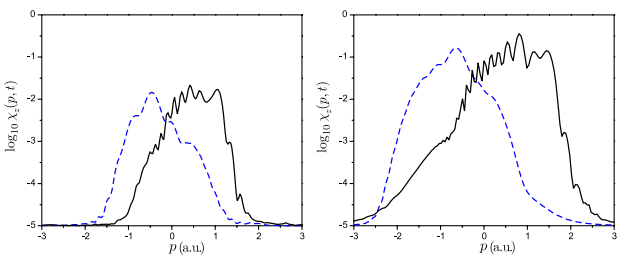

FIG. 2 (color online). The reduced one-dimensional momentum distribution $\chi_z(p, t)$ after the first half cycle (dashed lines) and after one cycle (solid lines) at $I = 10^{14}$ W/cm^2 (left) and 3×10^{14} W/cm^2 (right).

It is useful to compare laser-induced diffraction with diffraction of a Gaussian electron wave packet from an H_2^{2+} ion in the absence of laser field. To reveal the diffraction pattern in momentum space we calculate the ratio of one-dimensional momentum distributions in the two lateral directions—one along the molecular axis, the other perpendicular to it:

$$\mu(p, t) = \frac{\int |\Psi(p, p_y, p_z, t)|^2 dp_y dp_z}{\int |\Psi(p_x, p, p_z, t)|^2 dp_x dp_z}. \quad (4)$$

This ratio compensates for the sharp momentum falloff, common to both distributions, and reveals the diffraction pattern clearly.

The fact that the maxima and minima of $\mu(p, t)$ arise from diffraction is illustrated by the comparison in Fig. 3. We show a clear Cartesian space diffraction pattern produced by the Gaussian wave packet. We used a wave

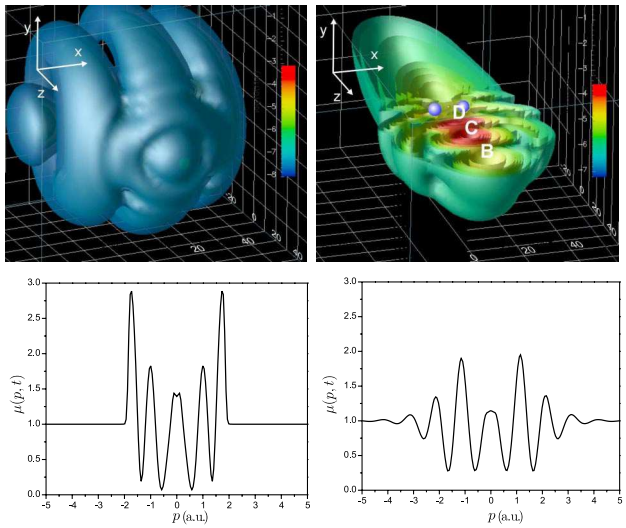

FIG. 3 (color online). The 3D electron density distributions (top) and the ratios of momentum distributions $\mu(p, t)$ (bottom). Left column shows the diffraction of a Gaussian wave packet with its initial momentum matching the effective cutoff momentum at $I = 3 \times 10^{14}$ W/cm^2; see details in text. Right column shows laser-induced diffraction at the same intensity and time $t = 55.2$. The labels **B**, **C**, and **D** in top right panel refer to the same wave packets as in Fig. 1. The image in the top right panel is clipped at $y = 0$. The electron density is plotted using a $\log_{10}$ scale.

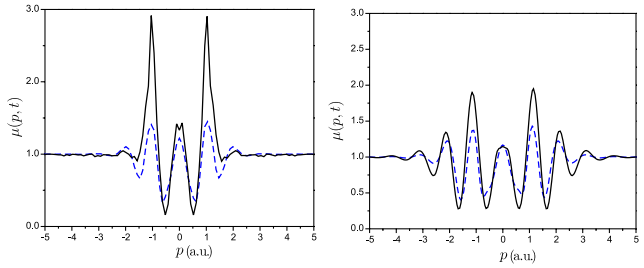

FIG. 4 (color online). The ratios of momentum distributions $\mu(p, t)$. The positions of the peaks are unchanged after the first half cycle (1/2 collision, dashed lines) and after one full cycle ($1^1/_2$ collision, solid lines) at $I = 10^{14}$ W/cm^2 (left) and 3×10^{14} W/cm^2 (right).

packet with the initial half-width of 8 Bohr and group velocity $v_0 = \pi/2$. The velocity is chosen to fit the diffraction ratio $\lambda_0/R = 4/6$. The 3D laser-induced diffraction pattern in Fig. 3 is not so obvious. The electron momentum spectra in the two cases are also quite different. Nevertheless, the Gaussian case leads to the same qualitative shape of $\mu(p, t)$ as the more complex laser-induced recollision diffraction process.

Figure 4 shows the shape of $\mu(p, t)$ for laser-induced diffraction at $I = 10^{14}$ and 3×10^{14} W/cm^2. The structure after one half cycle is due to two-center interference during the initial ionization process, while the enhancement of this structure after the full cycle is due to molecular diffraction of the recolliding electrons. The number of peaks in each case depends on the effective electron momentum value $p_{\max}$ in accordance with the diffraction rule. The separation between the peaks

$$\Delta p \approx 2\pi/R \tag{5}$$

gives an accurate measurement of the internuclear distance R.

In conclusion, diffractive information for aligned molecules is obtained from the ratio of the momentum distributions, projected onto two lateral directions. Viewed in this way, laser-induced electron diffraction is as simple as optical diffraction. This raises the intriguing possibility of whether laser-induced electron diffraction can be extended to more complex molecules.

Our 3D numerical approach can be used to answer this question. The model does not restrict the form of the molecular potential or the laser field polarization. Within the single active electron approximation, we can study many-electron molecules.

M. Yu. Ivanov, D. M. Villeneuve, and E. A. Shapiro are gratefully acknowledged for fruitful discussions. We are thankful to J. S. Tse and P. R. Bunker for their support. This work was supported in part by the Canadian National Research Council, British Council Science and Technology Fund.

*Electronic addresses: gennady.yudin@usherbrooke.ca; gennady.yudin@nrc.ca

[1] P. B. Corkum, Phys. Rev. Lett. **71**, 1994 (1993).
[2] T. Brabec, M. Yu. Ivanov, and P. B. Corkum, Phys. Rev. A **54**, R2551 (1996).
[3] G. L. Yudin and M. Yu. Ivanov, Phys. Rev. A **63**, 033404 (2001); **64**, 019902 (2001); **64**, 013409 (2001); **64**, 035401 (2001); V. R. Bhardwaj *et al.*, Phys. Rev. Lett. **86**, 3522 (2001).
[4] T. Zuo, A. D. Bandrauk, and P. B. Corkum, Chem. Phys. Lett. **259**, 313 (1996).
[5] H. Niikura *et al.*, Nature (London) **417**, 917 (2002); **421**, 826 (2003).
[6] M. Lein *et al.*, Phys. Rev. Lett. **88**, 183903 (2002); Phys. Rev. A **66**, 023805 (2002); M. Lein, J. P. Marangos, and P. L. Knight, Phys. Rev. A **66**, 051404 (2002).
[7] M. Lein *et al.*, Phys. Rev. A **67**, 023819 (2003); A. D. Bandrauk and H. Z. Lu, Phys. Rev. A **68**, 043408 (2003).
[8] M. Spanner *et al.*, J. Phys. B **37**, L243 (2004).
[9] M. Hentschel *et al.*, Nature (London) **414**, 509 (2001); P. M. Paul *et al.*, Science **292**, 1689 (2001).
[10] A. Baltuška *et al.*, Nature (London) **421**, 611 (2003).
[11] F. Légaré *et al.*, Phys. Rev. Lett. **91**, 093002 (2003).
[12] J. J. Larsen *et al.*, J. Chem. Phys. **111**, 7774 (1999); Phys. Rev. Lett. **85**, 2470 (2000).
[13] F. Rosca-Pruna and M. J. J. Vrakking, Phys. Rev. Lett. **87**, 153902 (2001).
[14] K. F. Lee *et al.*, J. Phys. B **37**, L43 (2004).
[15] I. V. Litvinyuk *et al.*, Phys. Rev. Lett. **90**, 233003 (2003); see also R. Velotta *et al.*, Phys. Rev. Lett. **87**, 183901 (2001).
[16] L.-Y. Peng *et al.*, J. Phys. B **36**, L295 (2003); J. Chem. Phys. **120**, 10046 (2004).
[17] A. D. Bandrauk and H. Z. Lu, in *Handbook of Numerical Analysis*, edited by P. G. Ciarlet and C. Le Bris (Elsevier Sciences, Amsterdam, 2003), Vol. 10, p. 803; K. Harumiya *et al.*, Phys. Rev. A **66**, 043403 (2002).
[18] D. Levesque and L. Verlet, J. Stat. Phys. **72**, 519 (1993).
[19] *Numerical Algorithms in Chemistry: Algebraic Methods*, edited by C. Moler and I. Shavitt (National Technical Information Service, Department of Commerce, Springfield, VA, 1978); M. L. Leininger *et al.*, J. Comput. Chem. **22**, 1574 (2001).
[20] E. R. Davidson, J. Comput. Phys. **17**, 87 (1975); B. Liu, *Numerical Algorithms in Chemistry: Algebraic Methods*, edited by C. Moler and I. Shavitt (National Technical Information Service, Department of Commerce, Springfield, VA, 1978), p. 49; J. H. van Lenthe and P. Pulay, J. Comput. Chem. **11**, 1164 (1990).